Chapter 6

Direct Ab Initio Dynamics Methods for Calculating Thermal Rates of Polyatomic Reactions

Thanh N. Truong, Wendell T. Duncan, and Robert L. Bell

Department of Chemistry, University of Utah, Salt Lake City, UT 84112

We present a direct *ab initio* dynamics methodology for calculating thermal rate constants from density functional theory (DFT). Dynamical theory is based on a variational transition state theory plus multi-dimensional semi-classical tunneling approximations. Potential energy surface information is calculated from a combined DFT/*ab initio* Molecular Orbital theory approach. We also present applications of this method to predicting detailed dynamics of a hydrogen abstraction reaction and proton transfer in a model biological system to illustrate its versility, accuracy and prospects for molecular modeling of reactive dynamics of polyatomic chemical reactions.

I. INTRODUCTION

The prediction of reaction rates from first principles allows one to make direct comparisons between theory and experiment and hence to deduce reaction mechanisms on the molecular level. For this reason, it has been a major goal of theoretical chemistry. However, it also has been a challenge particularly for polyatomic reactions for the following reasons. The conventional approach of reactive dynamical calculations using either the full quantal dynamics, classical or semiclassical trajectory method, or variational transition state theory (VTST) requires the availability of an accurate analytical potential energy function (PEF).[1-3] Developing such a potential energy function is not a trivial task and is a major obstacle for the

0097–6156/96/0629–0085$15.00/0

dynamical study of a new reaction despite the steady improvement in computer speed. This is because; i) the explicit functional form for a potential energy function is somewhat arbitrary and mostly depends on the investigator's intuition, ii) fitting this functional form to a set of *ab initio* energy points and any available experimental data is tedious and yet does not guarantee convergence or correct global topology, iii) the number of energy points needed grows geometrically with the number of geometrical internal coordinates. As the system size increases, this task becomes much more complex if it can still be accomplished at all. Thus, developments of new methodologies for studying dynamics, kinetics and mechanisms of large polyatomic reactions are of great interest.

Direct dynamics methods,[3-41] including those being developed in our lab[5,12,34-37] offer a viable alternative for studying chemical reactions of complex systems. In the direct dynamics approach, all required energies and forces for each geometry that is important for evaluating dynamical properties are obtained directly from electronic structure calculations rather than from empirical analytical force fields. Our earlier contributions to this area include the development of two different methodologies for calculating thermal rate constants and related properties. One approach is to estimate thermal rate constants and tunneling contributions using the interpolated Variational Transition State Theory (VTST) which has proven useful when available accurate *ab initio* electronic structure information is limited.[16] The other approach is to use a semiempirical molecular orbital Hamiltonian at the Neglect of Diatomic Differential Overlap (NDDO) level as a fitting function in which parameters have been readjusted to accurately represent activation barriers.[17] Full VTST calculations with multidimensional semiclassical tunneling approximations then can be carried out using this NDDO Hamiltonian with specific reaction parameters. Both of these approaches have been successfully applied to various chemical reactions.[16,17,23,24,26,32,39,42,43] However, many difficulties persist. For instance, in the former interpolated VTST approach, it is difficult to correlate vibrational modes in the transition state region to reactant and product asymptotes when mode crossings occur as they often do. In the later, it may prove to be difficult to adjust the original NDDO parameters to accurately describe the transition state region if the original NDDO potential energy surface differs significantly from the reference accurate *ab initio* surface. Recent development in combining both approaches[22,41] has some promise.

In this chapter, we will focus only on our recent contributions to the development of direct *ab initio* dynamics methods in which no experimental data other than physical constants were used for calculating thermal rate constants of gas-phase polyatomic reactions. The dynamical

method is based on full VTST theory plus multi-dimensional semiclassical tunneling corrections. The main difference with our previous work, however, is in the way the potential energy surface information is obtained. In our new approach, desired quantities are obtained directly from *ab initio* electronic structure calculations, thus no fitting is involved. For quantitative predictions of kinetic properties, the potential energy surface must be adequately accurate. If such information is to be calculated from a sufficiently accurate level of *ab initio* molecular orbital theory, the computational demand can be substantial. In this case, these methods are only useful for small systems, and thus they stop short of our goal. To alleviate this difficulty, we have introduced two new methodologies which can be used in combination. One is a focusing technique or an adaptive grid method in which more computational resources are spent on regions that are most sensitive to the dynamics and less resources elsewhere. This allows one to obtain an optimal accuracy with a minimum computational cost at a given level of theory. The other is the use of a computationally less demanding electronic structure method, density functional theory (DFT), for the computationally most expensive step in obtaining the potential energy information required for rate calculations. The later raises an interesting and important question. Would DFT methods be sufficiently accurate for this purpose?

Rapid developments in new functionals have significantly improved the accuracy of DFT methods in the past few years. Previously, most applications of DFT were for predicting properties of stable equilibrium structures.[44-46] Recently, more studies[47-53] on the accuracy of DFT methods for transition state properties have been reported. A general conclusion is that for transition state properties the non-local DFT and the hybrid DFT methods in which a portion of Hartree-Fock exchange is included yield results of comparable accuracy to the second-order Møller-Plesset (MP2) method but at a much cheaper computational cost, particulary for large systems. Thus, the computational advantage of DFT would allow application of the direct *ab initio* dynamics method to studying reactions involving larger polyatomic molecules.

To illustrate the applicability, accuracy and versatility of this direct *ab initio* dynamics approach, we present two different applications. One is the hydrogen abstraction $CH_4 + H <—> CH_3 + H_2$ reaction. This reaction has served as a prototype reaction involving polyatomic molecules and has played an important role in the theoretical and experimental developments of chemical kinetics. In addition, it has an intrinsic importance to combustion kinetics and is of fundamental interest to organic reaction mechanisms. For this reason, ample experimental rate data is available for comparison. Also this reaction is small enough so that

accurate *ab initio* MO calculations can also be performed to test the accuracy of DFT methods. The second example is the proton transfer in formamidine-water complex which has important implications in biological processes. Due to the limitted space, we can only focus on the accuracy of the methodology and not so much on the chemistry of these reactions. We refer readers to our original papers[5,34,35] for such discussion.

II. THEORY

A. Variational transition state theory

Variational transition state theory and multidimensional semiclassical tunneling methods have been described in detail elsewhere.[54-60] In this chapter, we only capture the essence of the theory and the approximations involved in the applications presented here. VTST is based on the idea that by varying the dividing surface along the minimum energy path (MEP) to minimize the rate, one can minimize the error due to "recrossing" trajectories. The MEP is defined as the steepest descent path from the saddle point to both the reactant and product directions in the mass-weighted cartesian coordinate system. The reaction coordinate *s* is then defined as the distance along the MEP with the origin located at the saddle point and is positive on the product side and negative on the reactant side. For a canonical ensemble at a given temperature T, the canonical variational theory (CVT) rate constant for a bimolecular reaction is given by

$$k^{CVT}(T) = \min_{s} k^{GT}(T,s) \tag{1}$$

where

$$k^{GT}(T,s) = \frac{\sigma}{\beta h}\frac{Q^{GT}(T,s)}{\Phi^{R}(T)} e^{-\beta V_{MEP}(s)}. \tag{2}$$

In these equations, $k^{GT}(T,s)$ is the generalized transition state theory rate constant at the dividing surface which intersects the MEP at *s* and is orthogonal to the MEP at the intersection point. σ is the symmetry factor accounting for the possibility of more than one symmetry-related reaction path and can be calculated as the ratio of the product of the reactant rotational symmetry numbers to the transition state one. For example, the rotational symmetry numbers for CH_4 (T_d), CH_3 (D_{3h}), H_2 ($D_{\infty h}$) and the $H_3C..H..H$ generalized transition state (C_{3v}) are 12, 6, 2 and 3, respectively. Consequently, σ equals 4 for both the forward and reverse directions of the

$CH_4 + H \leftrightarrow CH_3 + H_2$ reaction. β is $(k_BT)^{-1}$ where k_B is Boltzman's constant and h is Planck's constant. $\Phi^R(T)$ is the reactant partition function (per unit volume for bimolecular reactions). $V_{MEP}(s)$ is the classical potential energy (also called the Born-Oppenheimer potential) along the MEP with its zero of energy at the reactants, and $Q^{GT}(T,s)$ is the internal partition function of the generalized transition state at *s* with the local zero of energy at $V_{MEP}(s)$. Both $\Phi^R(T)$ and $Q^{GT}(T,s)$ partition functions are approximated as products of electronic, vibrational and rotational partition functions. For the electronic partition function, the generalized transition state electronic excitation energies and degeneracies are assumed to be the same as at the transition state. For rotations, since the rotational energy levels are generally closely spaced, replacing the quantal rotational partition functions by the classical ones yields very little loss in accuracy. For vibrations, in the present study, the partition functions are calculated quantum mechanically within the framework of the harmonic approximation. Note that anharmonicity sometimes can have a noticeable effect on reaction rates particularly at higher temperatures. However, it is not included in the applications presented below.

The canonical variational transition state theory described above yields the hybrid (i.e. classical reaction path motion with vibrational degrees of freedom quantized) rate constants. Furthermore, if the generalized transition state is located at the saddle point (*s*=0), eq. (2) reduces to conventional transition state theory.

To include quantal effects for motion along the reaction coordinate, we multiply the CVT rate constants by a transmission coefficient, κ (T). Thus, the final quantized rate constant is

$$k(T) = \kappa^{CVT/G}(T) k^{CVT}(T) \tag{3}$$

B. Multidimensional Semiclassical Tunneling Methods

To calculate the transmission coefficient, we first approximate the effective potential for tunneling to be the vibrationally adiabatic ground-state potential curve defined by

$$V_a^G(s) = V_{MEP}(s) + \varepsilon_{\text{int}}^G(s) \tag{4}$$

where $\varepsilon_{\text{int}}^G(s)$ denotes the zero-point energy in vibrational modes tranverse to the MEP. The ground state transmission coefficient, $\kappa^{CVT/G}(T)$, is then approximated as the ratio of the thermally averaged

multidimentional semiclassical ground-state transmission probability, $P^G(E)$, for reaction in the ground state to the thermally averaged classical transmission probability for one-dimensional scattering by the ground-state effective potential $V_a^G(s)$.[24,56-65] If we denote the CVT transition state for temperature T as $s_*^{CVT}(T)$, the value of $V_a^G\left\{s_*^{CVT}(T)\right\}$, denoted as $E_*(T)$, is the quasiclassical ground-state threshold energy, then the transmission coefficient $\kappa^{CVT/G}(T)$ can be expressed as

$$\kappa^{CVT/G}(T) = \frac{\int_0^\infty P^G(E) e^{-E/k_bT} dE}{\int_{E_*(T)}^\infty e^{-E/k_bT} dE}. \tag{5}$$

The semiclassical transmission probability $P^G(E)$ accounts for both nonclassical reflection at energies above the quasiclassical threshold and also nonclassical transmission, i.e., tunneling, at energies below that threshold. However, the Boltzmann factor in Eq. (5) makes tunneling the far more important contribution.

Several approximations for the semiclassical transmission probability $P^G(E)$ are available, however, only two, namely, the zero-curvature[58] and the centrifugal-dominant small-curvature semiclassical adiabatic ground-state[65] approximations used in the present study are presented here. For convenience, we label them as ZCT and SCT for the zero-curvature tunneling and small-curvature tunneling cases, respectively. Since the ZCT approximation is a special case of the SCT approximation, we present only the formalism for the SCT below.

The SCT used here is a generalization of the Marcus-Coltrin approximation in which the tunneling path is distorted from the MEP out to the concave-side vibrational turning point in the direction of the internal centrifugal force. This phenomenon is commonly refered to as "corner cutting". Instead of defining the tunneling path explicitly, the centrifugal effect is included by replacing the reduced mass by an effective reduced mass, $\mu_{eff}(s)$, which is used to evaluate imaginary action integrals and thereby tunneling probabilities. Note that in the mass-weighted cartesian coordinate system, the reduced mass μ is set equal to 1 amu. The ground-state transmission probability at energy E is

$$P^G(E) = \frac{1}{\left\{1 + e^{-2\theta(E)}\right\}} \tag{6}$$

where θ(E) is the imaginary action integral evaluated along the tunneling path,

$$\theta(E) = \tfrac{2\pi}{h} \int_{s_l}^{s_r} \sqrt{2\mu_{eff}(s)\left|E - V_a^G(s)\right|}\, ds \tag{7}$$

and where the integration limits, s_l and s_r, are the reaction-coordinate turning points defined by

$$V_a^G\left[s_l(E)\right] = V_a^G\left[s_r(E)\right] = E \tag{8}$$

Note that the ZCT results can be obtained by setting $\mu_{eff}(s)$ equal to μ in Eq. (7). The effect of the reaction-path curvature is included in the effective reduced mass $\mu_{eff}(s)$ which is given by

$$\mu_{eff}(s) = \mu \times \min\begin{Bmatrix} \exp\left\{-2\bar{a}(s) - [\bar{a}(s)]^2 + \left(d\bar{t}/ds\right)^2\right\} \\ 1 \end{Bmatrix} \tag{9}$$

where

$$\bar{a}(s) = \left|\kappa(s)\bar{t}(s)\right| \tag{10}$$

The magnitude of the reaction-path curvature κ (s) is given by

$$\kappa(s) = \left(\sum_{m=1}^{3N-7} \left[\kappa_m(s)\right]^2 \right)^{1/2} \tag{11}$$

where the summation is over all 3N-7 generalized normal modes and $\kappa_m(s)$ is the reaction-path curvature component along mode m given by[66]

$$\kappa_m(s) = -\mathbf{L}_m^T \mathbf{F} \frac{\nabla V}{|\nabla V|^2} \tag{12}$$

and where $\mathbf{L}_m^T$ is the transpose of the generalized normal mode eigenvector of mode m, **F** is the force constant matrix (Hessian matrix),

∇V is the gradient. Finally, $\bar{t}(s)$ is the maximum concave-side vibrational displacement along the curvature direction for which there is no tunneling in the vibrational coordinates. Within the harmonic approximation, $\bar{t}(s)$ is given by

$$\bar{t}(s)=\left(\frac{\kappa\hbar}{\mu}\right)^{1/2}\left\{\sum_{m}^{F-1}\left[\kappa_m(s)\right]^2 w_m^2(s)\right\}^{-1/4} \tag{13}$$

where w_m is the generalized vibrational frequency of mode m.

As described above, in order to carry out full VTST calculations and multi-dimensional semiclassical zero- or small-curvature tunneling corrections, geometries, energies, gradients and Hessians are needed at the stationary points and along the MEP. Hessian calculations along the MEP are computationally the most expensive step. Below we describe two different methodologies for minimizing the computational cost of this step.

C. Focusing technique

The focusing technique was developed to assure the convergence of the calculated rate constants with a minimal number of Hessians required. This method involves two separate steps. First, a preliminary rate calculation with a coarse Hessian grid is carried out to estimate regions containing the temperature-dependent canonical transition states or those having large curvature where the "corner cutting" effect would be large. A finer Hessian grid is then used for these regions to improve the accuracy of the calculated CVT rate constants and the SCT tunneling probability. The technique will be illustrated in more detail below.

D. Employing DFT methods

Non-local DFT methods such as the combination of Becke's Half-and-Half[67] (BH&H) or three parameter[68] (B3) hybrid exchange with Lee-Yang-Parr[69] (LYP) correlation functionals can be used to calculate the geometries and Hessians along the MEP. The hybrid BH&H functional as implemented in the G92/DFT program[70] consists of 50% Hartree-Fock and 50% Slater exchange contribution. The DFT energies, however, are not always sufficiently accurate. In this case, to obtain more a accurate potential energy along the MEP, one can either perform a series of single point calculations at a more accurate level of theory with a larger basis set

for selected points along the MEP or scale $V_{MEP}(s)$ by a constant factor to match a more accurately calculated classical barrier and reaction energy.

From our experience, we have found that the B3LYP method is slightly more accurate than the BH&HLYP method for calculating equilibrium structures. For finding transition state structures, the BH&HLYP method has shown to be more reliable for open-shell sytems. For closed-shell systems, our preliminary results indicate that both B3LYP and BH&HLYP are adequate. In practice, we often carry out accurate *ab initio* MO calculations at the stationary points to check the accuracy of DFT methods prior to their use in rate calculations.

III. APPLICATIONS

A. $CH_4 + H <—> CH_3 + H_2$ reaction

We used this reaction as a test case where the reaction valley (geometries, energies, gradients and Hessians along the MEP) was calculated with both the Quadratic Configuration Interaction including all Single and Double excitations (QCISD) and the hybrid BH&HLYP methods. Both methods use the same 6-311G(d,p) basis set. In particular, we have performed a new benchmark converged direct *ab initio* dynamics rate calculations for this reaction. In the new calculations, the reaction path was calucated at the QCISD/6-311G(d,p) with the step size of 0.01 $amu^{1/2}$bohr which is an order of magnitude smaller than in our previous study.[34] Hessian grids are also much finer. Furthermore, instead of scaling the potential energy along the MEP as in the previous study, single point PMP4/6-311+G(2df,2pd) calculations were performed at the Hessian grids.

Reaction energies and barrier heights are listed in Table 1. The BH&H-LYP classical barriers were found to be too low by 2.7 and 0.6 kcal/mol for the forward and reverse reactions, respectively, as compared to the CCSD(T)/cc-pVQZ results. Single-point spin projected fourth-order Møller-Plesset perturbation theory (PMP4) calculations with the larger 6-311+G(2df,2pd) basis set at the BH&H-LYP/6-311G(d,p) geometries bring the differences in the classical barriers to less than 0.7 kcal/mol and also yield the reaction enthalpy at 0 K to be -0.36 kcal/mol as compared to the CCSD(T)/cc-pVQZ value of -0.3 kcal/mol and the experimental value from JANAF tables[74] of -0.02 kcal/mol.

Table 1: Heat of reaction and barrier heights[a] (kcal/mol) for the CH_4 +H <--> CH_3 +H_2 reaction

Level	ΔE	ΔH_0^0	$\Delta V_f^{\ddagger}$	$\Delta V_r^{\ddagger}$
BH&HLYP/6-311G(d,dp)	1.4	-1.9	12.6 (e11.1)[a]	11.2 (13.0)[a]
PMP4/6-311+G(2df,2pd) //BH&HLYP/6-311G(d,p)	2.9	-0.4	14.6 (13.1)	11.7 (13.5)
QCISD/6-311G(d,p)	2.5	-0.7	16.3 (14.8)	13.8 (15.5)
PMP4/6-311+G(2df,2pd) //QCISD/6-311G(d,p)	3.6	0.3	14.6 (13.0)	10.9 (12.7)
CCSD(T)/cc-pVQZ //CCSD(T)/cc-VQZ[b]	3.5	-0.3	15.3 (13.1)	11.8 (13.3)
J3[c]	2.8	-0.02	12.9 (11.8)	10.1 (11.9)
Expt.[d]	2.6[d]	-1.3[d] -0.02[e]	(13.3 ± 0.5)[d]	(14.6 ± 0.4)[d]

[a] Zero-point energy corrected barriers are given in the parentheses.
[b] From Ref. 71.
[c] From Ref. 72.
[d] From Ref. 73.
[e] From Ref. 74.

Similar results were obtained if the QCISD geometries were used in the PMP4 calculations except the calculated reaction enthalpy is slightly positive. Using the BH&H-LYP zero-point energy correction, the PMP4//BH&H-LYP zero-point energy corrected barriers for both forward and reverse reactions are within 0.2 kcal/mol of the CCSD(T)/cc-pVQZ values and are also in good agreement with experimental data.[73]

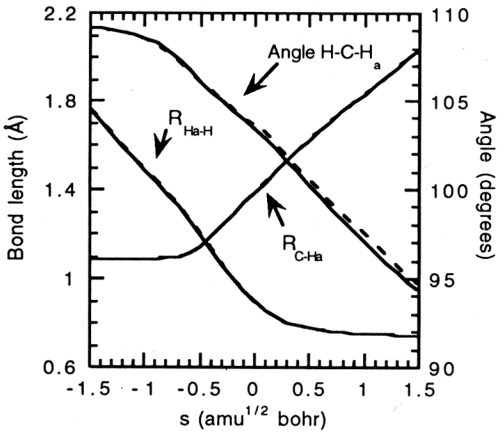

Figure 1: BH&HLYP (solid lines) and QCISD (dased lines) geometrical parameters along the MEP of the H + CH_4 —>H_2 + CH_3 reaction vs the reaction coordinate s.

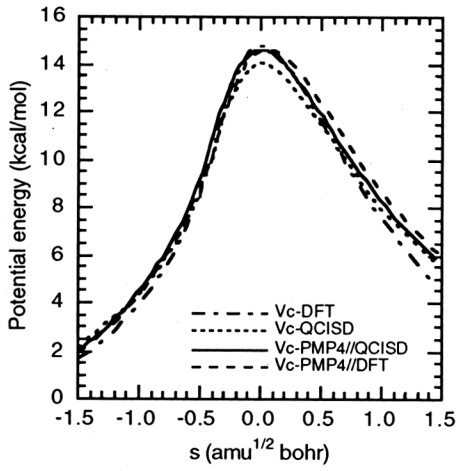

Figure 2: Classical potential energy curves { PMP4// QCISD (solid), PMP4//BH&HLYP (dashed), scaled BH&HLYP (dashed-dotted), scaled QCISD (dotted)}.

The geometries along the minimum energy path calculated by both the BH&H-LYP and QCISD levels are shown in Figure 1. We found that the BH&H-LYP method yields the active C-H_a and H_a-H bond lengths and H-C-H_a angle as functions of the reaction coordinate in excellent agreement with the QCISD results. More specifically, Figure 1 shows an unnoticeable difference in the active bond lengths and a difference of less than 1 degree in the H-C-H_a angle between the two methods.

The good agreement between PMP4//QCISD and PMP4//BH&HLYP potential curves as shown in Fig. 2 indicates that the accuracy of the potential energy along the MEP can be improved by carrying out single point PMP4/6-311+G(2df,2pd) calculations at selected points along the DFT MEP. When such single point calculations on the Hessian grids are computationally expensive, it is possible to scale the potential energy along the MEP by a constant factor to adjust the barrier height to more accurate calculations. As shown in Fig. 2, we scaled the BH&HLYP and QCISD potential curves to best reproduce both the forward

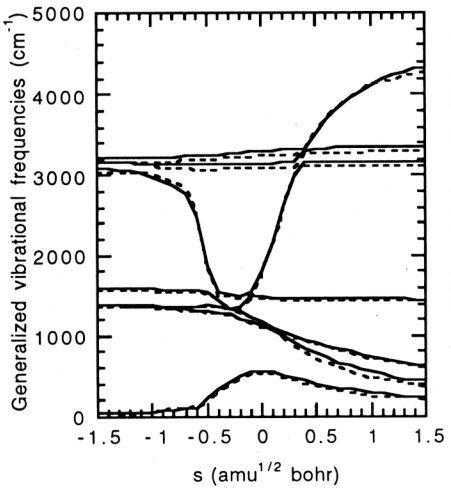

Figure 3: BH&HLYP (solid lines) and QCISD (dashed lines) harmonic frequencies along the reaction coordinate s.

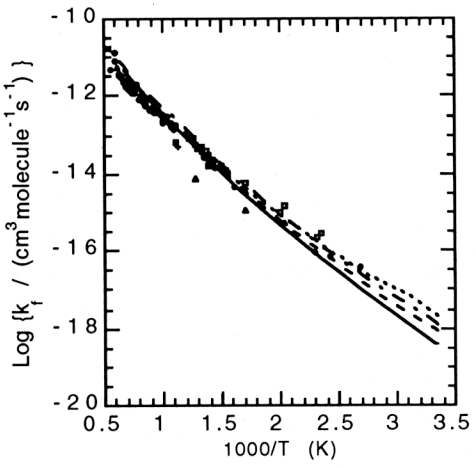

Figure 4: Arrhenius plot for the forward H + CH_4 reaction. Symbols are experimental data. Lines are the CVT/SCT results {PMP4//QCISD (solid), PMP4//BH&HLYP (dashed), scaled BH&HLYP (dotted), scaled QCISD (dashed-dotted)}.

and reverse classical barriers calculated at the CCSD(T)/cc-pVQZ level of theory by Kraka et al.[71] Note that both the scaled DFT and QCISD classical potential curves have about the same width compared to the PMP4//QCISD curves, though the barrier heights differ by about 1 kcal/mol. In general, scaling the reaction profile by a constant to obtain more accurate barrier heights does not guarantee to improve the shape as well as the asymtotic regions of the reaction profile. It is possible, however, to add a small number of single point calculations as discussed above and to interpolate the energy corrections along the MEP. Such a procedure is now being tested in our lab.

Generalized frequencies calculated at the BH&H-LYP/6-311G(d,p) level versus the reaction coordinate are plotted in Figure 3 along with the previous QCISD/6-311G(d,p) results. Note that excellent agreement was found between the BH&H-LYP and QCISD results, though the former are slightly larger by about 3%.

The Ahrrenius plots of the calculated and experimental forward and reverse rate constants are

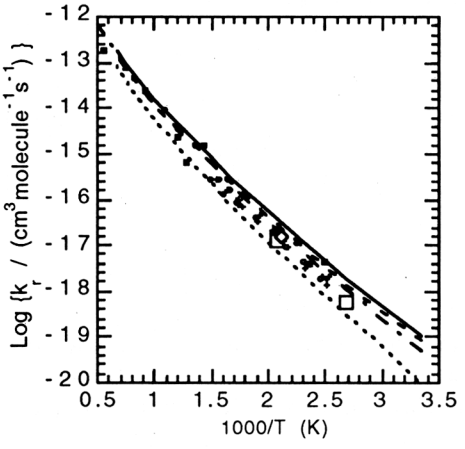

Figure 5: Arrhenius plot of the $CH_3 + H_2$ reaction. Symbols are experimental data. Lines are the CVT/SCT results {PMP4//QCISD (solid), PMP4//BH&HLYP(dashed), scaled BH&HLYP (dotted), scaled QCISD (dashed-dotted)}.

shown in Figures 4 and 5, respectively. Note that our CVT/SCT-PMP4//BH&H-LYP results for the forward rate constants are in excellent agreement with the experimental data for the temperature range from 300-1500 K with the largest deviation factor of 1.5 compared to the recent recommended experimental values.[75] Similar results were found for the PMP4//QCISD calculations. The deviation factor is slightly larger for the reverse rate constants from both the PMP4//QCISD and PMP4//BH&HLYP calculations, particularly ranging from 2.5-3.0 for the temperature range from 300-1500 K. Rate constants calculated from the scaled BH&HLYP and QCISD potential are also in reasonably good agreement with the experimental data.

The above results show that we can use computationally less demanding DFT methods to provide geometries and Hessians along the MEP. DFT energies may not be sufficient for rate calculations, however, potential energies along the MEP can be improved by scaling by a factor to reproduce classical forward and/or reverse barriers from more accurate calculations or performing a series of single point calculations at a more accurate *ab initio* MO level.

B. Proton transfer in formamidine-water complex

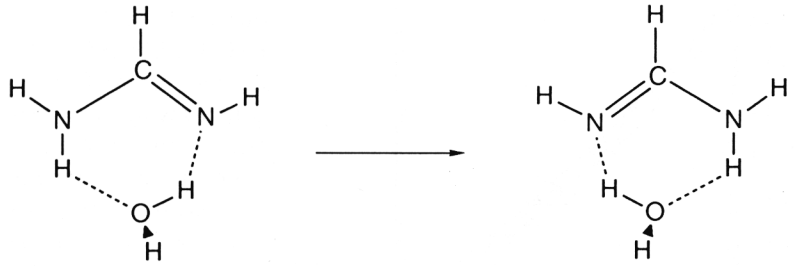

We used proton transfer in the formamidine-water complex as a basic model for studying proton transfer in hydrogen bonded systems, though formamidine and its amidine class also have their own biological and pharmaceutical importance.

Previous studies[5,76] found that adding a water molecule to bridge the proton donor and acceptor sites stabilizes the transition state. This lowers the barrier by 27 kcal/mol, and as a consequence, significantly enhances the transfer rate. Due to the small proton mass, we also found that the tunneling contribution is significant, particularly at low temperatures, by comparing the CVT and CVT/SCT results. Furthermore, the "corner cutting" effect included in the CVT/SCT calculations on the multidimensional surface greatly enhances the tunneling probability for proton transfer in the formamidine-water complex (see Figure 6). This is illustrated by the large increase in the CVT/SCT rate constants when compared to the CVT/ZCT rate. Note that in ZCT calculations, tunneling is restricted to be along the MEP. The reaction valley in this case was calculated at the MP2 level. The potential energy along the MEP was further scaled by a factor of 1.123 to match the

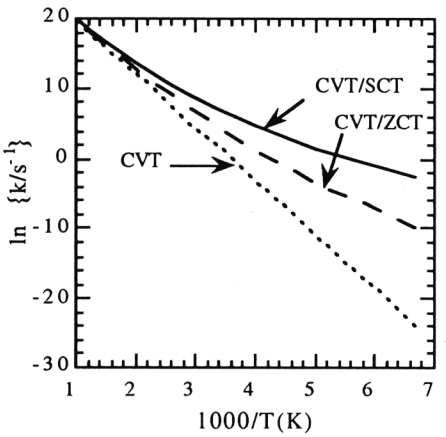

Figure 6: Arrhenius plot of calculated CVT, CVT/ZCT and CVT/SCT thermal rate constants. (Adapted from Ref. 5).

CCSD(T)//MP2 classical barrier heights. In all *ab initio* MO and DFT calculations for this system, the 6-31G(d,p) basis set was used.

The large "corner cutting" tunneling effect requires much more potential energy surface information than just in the vicinity of the saddle point. However, due to the size of this system, one would like to minimize the number of MP2 Hessian calculations without a significant loss to the accuracy. Thus, it is a good example to illustrate the accuracy of our focusing technique described below.

For this discussion, the MEP was calculated at the MP2 level with a maximum of 28 Hessian points evenly distributed between s values of 0 and 1.2 $amu^{1/2}bohr$. Due to the symmetry of the MEP, this is equivalent to a total of 59 Hessian points, including three stationary points, for the entire MEP. Using the CVT/SCT thermal rate constants calculated from these 28 calculated Hessian points as the reference point, we have calculated CVT/SCT rate constants with the number of Hessian points less than the full 28, which were chosen by the focusing technique, and plotted in Figure 7 with the percent difference in the rate constant at 300 K versus the number of Hessians used. We found that a minimum of 10 Hessian points is required for the convergence of the rate constant to within 10%. Furthermore, using a low-pass filtering technique to remove noise in the calculated effective reduced mass slightly improves this convergence. Note that even with 5 Hessian points, the calculated rate constant at 300 K converges to within a factor of two in the 28-point case. For reactions with a smaller tunneling contribution than this case, a smaller number of Hessians may be sufficient. In addition, not including the "corner cutting" effect from the bending modes, i.e. vibrational modes with frequency less than 1800 cm^{-1}, only introduces an error of less than 20%.

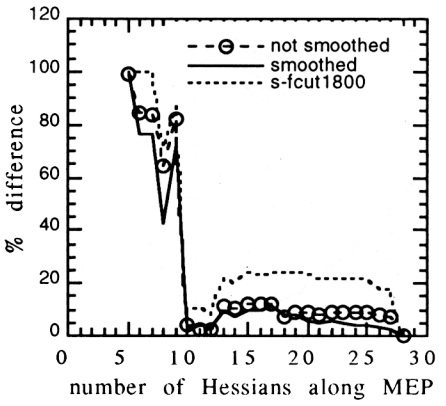

Figure 7: Convergence of the calculated rate constant at 300 K as functions of the number of Hessians along the MEP. (Adapted from Ref. 5)

Finally, using the MP2 rate results for the tautomerization in the formamidine-water complex

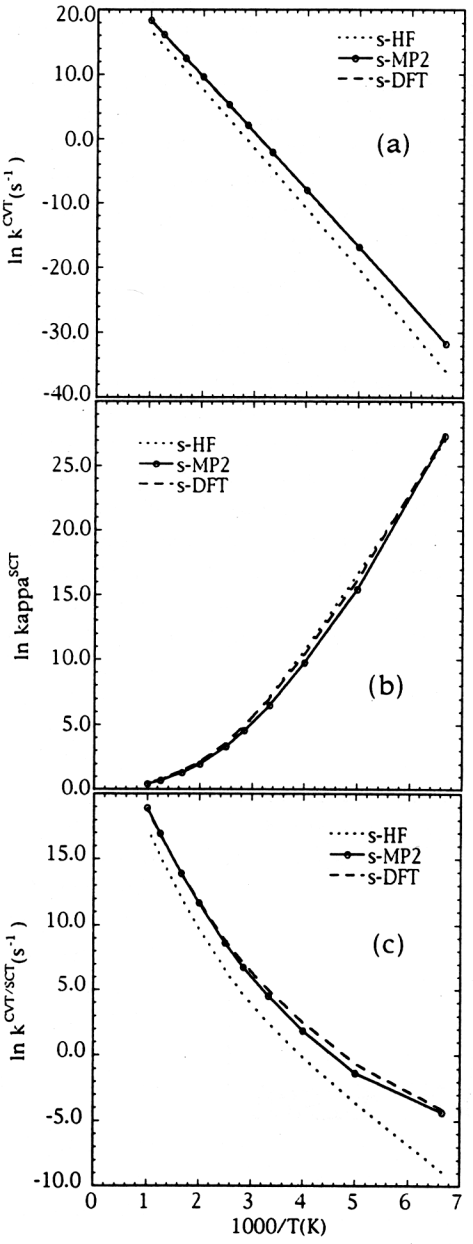

Figure 8: Arrhenius plots of the individual contributions, (a) CVT rate, (b) SCT transmission coefficients, and (c) the total CVT/SCT rate constants vs 1000/T (K). (Adapted from Ref. 5.)

as a reference point, we have investigated the accuracy using the non-local BH&H-LYP DFT method for calculating the potential energy information. In this case, we also used the same barrier scaling procedure described above. In addition, we also investigated another computationally less demanding approach. That is to use HF theory, but in addition to scaling the classical barrier to the CCSD(T)//MP2 value, the HF frequencies were also scaled by a factor of 0.9. In both HF and DFT cases, the MEP's were calculated with the same step size of 0.1 $amu^{1/2}bohr$ as used in the MP2 calculations. The Arrhenius plot for the MP2, HF and DFT CVT and CVT/SCT rate constants are also shown in Figure 8. We found the HF-CVT rate constants are noticeably smaller than the MP2 and DFT rates. As a result, the final HF CVT/SCT rate constants are also smaller and the differences increase as the temperature decreases. The excellent agreement between the MP2 and DFT rate constants further supports the above conclusion on the use of non-local DFT methods for direct *ab initio* dynamics calculations. For instance at 300 K, the HF rate constant is smaller than the MP2 value by a factor of 8.0 while the DFT rate constant is larger by a factor of 1.6.

We have further developed these direct *ab initio* dynamics methods to calculate vibrational-state selected rates of polyatomic reactions.[12,37] The results so far are encouraging. Particularly, it allows one to correlate features on the potential surface to state specific chemistry. Thermal and vibrational-state selected rate constants of polyatomic reactions now can be routinely calculated from *ab initio* MO and/or DFT methods by using our TheRate (Theoretical Rate) program.[77] We are in the process of developing new methodologies for including anharmonicity and large curvature tunneling contributions within our direct *ab initio* dynamics approach.

IV. CONCLUSION

The direct *ab initio* dynamics method we described above with the use of a non-local DFT method to provide potential energy information and a focusing technique to minimize the number of Hessians required offers a promissing alternative for studying kinetics, dynamics and mechanisms of large polyatomic reactions. Within the same methodology, one can further extend the dynamical theory to treat chemical reactions on crystal surfaces as well as in solutions. Such steps are now being taken in our lab.

Acknowledgement

This work was supported in part by the University of Utah and by the National Science Foundation through an NSF Young Investigator Award to T.N.T..

References

[1]G. C. Schatz, *Rev. Mod. Phys.* **61,** 669 (1989).

[2]*Potential Energy Surfaces and Dynamics Calculations*, Vol. , edited by D. G. Truhlar (Plenum, New York, 1981).

[3]D. G. Truhlar, M. S. Gordon, and R. Steckler, *Chem. Rev.* **87,** 217 (1987).

[4]K. K. Baldridge, M. S. Gordon, D. G. Truhlar, and R. Steckler, *J. Phys. Chem.* **93,** 5107 (1989).

[5]R. Bell and T. N. Truong, *J. Chem. Phys.* **101,** 10442 (1994).

[6]B. Calef and A. Redondo, *Chem. Phys. Letters* **223,** 1 (1994).

[7]R. Car and M. Parrinello, *Phys. Rev. Lett.* **55,** 2471 (1985).

[8]R. Car and M. Parrinello, in *Simple Molecular Systems at Very High Density*, edited by A. Polian, P. Loubeyre, and N. Boccara (Plenum, New York, 1989), pp. 455.

[9]W. Chen, W. L. Hase, and H. B. Schlegel, *Chem. Phys. Letters* **228,** 436 (1994).

[10]S. M. Colwell and N. C. Handy, *J. Chem. Phys.* **82,** 1281 (1985).

[11]C. J. Doubleday, J. W. J. McIver, and M. Page, *J. Phys. Chem.* **92,** 4367 (1988).

[12]W. T. Duncan and T. N. Truong, *J. Chem. Phys.* **103,** 9642 (1995).

[13]M. J. Field, *Chem. Phys. Lett.* **172,** 83 (1990).

[14]B. C. Garrett, M. L. Koszykowski, C. F. Melius, and M. Page, *J. Phys. Chem.* **94,** 7096 (1990).

[15]B. C. Garrett and C. F. Melius, in *Theoretical and Computational Models for Organic Chemistry*, edited by S. J. Formosinho, I. G. Csizmadia, and L. G. Arnaut (Kluwer, Dordrecht, 1991), pp. 25-54.

[16]A. Gonzalez-Lafont, T. N. Truong, and D. G. Truhlar, *J. Chem. Phys.* **95,** 8875 (1991).

[17]A. Gonzalez-Lafont, T. N. Truong, and D. G. Truhlar, *J. Phys. Chem.* **95,** 4618 (1991).

[18]S. K. Gray, W. H. Miller, Y. Yamagychi, and H. F. Schaefer, *J. Am. Chem. Soc.* **103,** 1900 (1981).

[19]J. C. Greer, R. Ahlrichs, and I. V. Hertel, *Z. Phys. D - Atoms, Molecules and Clusters* **18,** 413 (1991).

[20]B. Hartke and E. A. Carter, *J. Chem. Phys.* **97,** 6569 (1992).

[21]T. Helgaker, E. Uggerud, and H. J. A. Jensen, *Chem. Phys. Lett.* **173,** 145 (1990).

[22]W.-P. Hu, Y.-P. Liu, and D. G. Truhlar, *J. Chem. Soc. Faraday Trans.* **90,** 1715 (1994).

[23]Y.-P. Liu, G. C. Lynch, T. N. Truong, D.-h. Lu, and D. G. Truhlar, *J. Am. Chem. Soc.* **115,** 2408 (1993).

[24]Y.-P. Liu, D.-h. Lu, A. Gonzalez-Lafont, D. G. Truhlar, and B. C. Garrett, *J. Am. Chem. Soc.* **115,** 7806 (1993).

[25]D. Malcome-Lawes, *J. Amer. Chem. Soc. Faraday Trans. 2* **71,** 1183 (1975).

[26]V. S. Melissas and D. G. Truhlar, *J. Phys. Chem.* **98,** 875 (1994).

[27]K. Moroduma and S. Kato, in *Potential Energy Surfaces and Dynamics Calculations*, edited by D. G. Truhlar (Plenum, New York, 1981), pp. 243-264.
[28]D. K. Remler and P. A. Madden, *Mol. Phys* **70,** 921 (1990).
[29]A. Tachibana, I. Okazaki, M. Koizumi, K. Hori, and T. Yamabe, *J. Am. Chem. Soc.* **107,** 1190 (1985).
[30]A. Tachibana, H. Fueno, and T. Yamabe, *J. Am. Chem. Soc.* **108,** 4346 (1986).
[31]D. G. Truhlar and M. S. Gordon, *Science* **249,** 491 (1990).
[32]T. N. Truong and D. G. Truhlar, *J. Chem. Phys.* **93,** 1761 (1990).
[33]T. N. Truong and J. A. McCammon, *J. Am. Chem. Soc.* **113,** 7504 (1991).
[34]T. N. Truong, *J. Chem. Phys.* **100,** 8014 (1994).
[35]T. N. Truong and W. T. Duncan, *J. Chem. Phys.* **101,** 7408 (1994).
[36]T. N. Truong and T. J. Evans, *J. Phys. Chem.* **98,** 9558 (1994).
[37]T. N. Truong, *J. Chem. Phys.* **102,** 5335 (1995).
[38]E. Uggerud and T. Helgaker, *J. Am. Chem. Soc.* **114,** 4265 (1992).
[39]A. A. Viggiano, J. Paschekewitz, R. A. Morris, J. F. Paulson, A. Gonzalez-Lafont, and D. G. Truhlar, *J. Am. Chem. Soc.* **113,** 9404 (1991).
[40]I. Wang and M. J. Karplus, *J. Am. Chem. Soc.* **95,** 8160 (1973).
[41]D. G. Truhlar, in *The Reaction Path in Chemistry: Current Approaches and Perspectives*, edited by D. Heidrich (Kluwer Academic, 1995), pp. 229.
[42]V. S. Melissas and D. G. Truhlar, *J. Chem. Phys.* **99,** 3542 (1993).
[43]V. S. Melissas and D. G. Truhlar, *J. Chem. Phys.* **99,** 1013 (1993).
[44]J. Andzelm and E. Wimmer, *J. Chem. Phys.* **96,** 1280 (1992).
[45]B. G. Johnson, P. M. W. Gill, and J. A. Pople, *J. Chem. Phys.* **98,** 5612 (1993).
[46]*Density Functional Methods in Chemistry*, Vol. , edited by J. K. Labanowski and J. W. Andzelm (Springer-Verlag, New York, 1991).
[47]Y. Abashkin and N. Russo, *J. Chem. Phys.* **100,** 4477 (1994).
[48]R. V. Stanton and K. M. Merz, Jr., *J. Chem. Phys.* **100,** 434 (1994).
[49]Q. Zhang, R. Bell, and T. N. Truong, *J. Phys. Chem.* **99,** 592 (1995).
[50]J. Baker, J. Andzelm, M. Muir, and P. R. Taylor, *Chem. Phys. Letters* **237,** 53 (1995).
[51]T. Ziegler, *Chem. Rev.* **91,** 651 (1991).
[52]L. Fan and T. Ziegler, *J. Chem. Phys.* **92,** 3645 (1990).
[53]L. Y. Fan and T. Ziegler, *J. Am. Chem. Soc.* **114,** 3823 (1992).
[54]B. C. Garrett and D. G. Truhlar, *J. Chem. Phys.* **70,** 1593 (1979).
[55]D. G. Truhlar and B. C. Garrett, *Accounts Chem. Res.* **13,** 440 (1980).
[56]D. G. Truhlar, A. D. Isaacson, R. T. Skodje, and B. C. Garrett, *J. Phys. Chem.* **86,** 2252 (1982).
[57]D. G. Truhlar and B. C. Garrett, *Annu. Rev. Phys. Chem.* **35,** 159 (1984).
[58]D. G. Truhlar, A. D. Isaacson, and B. C. Garrett, in *Theory of Chemical Reaction Dynamics*, Vol. 4, edited by M. Baer (CRC Press: Boca Raton, Florida, 1985), pp. 65-137.

[59]D. G. Truhlar and B. C. Garrett, *J. Chim. Phys.* **84,** 365 (1987).
[60]S. C. Tucker and D. G. Truhlar, in *New Theoretical Concepts for Understanding Organic Reactions*, edited by J. Bertran and I. G. Csizmadia (Kluwer, Dordrecht, Netherlands, 1989), pp. 291-346.
[61]B. C. Garrett, N. Abushalbi, D. J. Kouri, and D. G. Truhlar, *J. Chem. Phys.* **83,** 2252 (1985).
[62]M. M. Kreevoy, D. Ostovic, D. G. Truhlar, and B. C. Garrett, *J. Phys. Chem.* **90,** 3766 (1986).
[63]A. D. Isaacson, B. C. Garrett, G. C. Hancock, S. N. Rai, M. J. Redmon, R. Steckler, and D. G. Truhlar, *Computer Phys. Comm.* **47,** 91 (1987).
[64]B. C. Garrett, T. Joseph, T. N. Truong, and D. G. Truhlar, *Chem. Phys.* **136,** 271 (1989).
[65]D.-h. Lu, T. N. Truong, V. S. Melissas, G. C. Lynch, Y. P. Liu, B. C. Garrett, R. Steckler, A. D. Isaacson, S. N. Rai, G. C. Hancock, J. G. Lauderdale, T. Joseph, and D. G. Truhlar, *Computer Phys. Comm.* **71,** 235 (1992).
[66]M. Page and J. W. McIver Jr., *J. Chem. Phys.* **88,** 922 (1988).
[67]A. D. Becke, *J. Chem. Phys.* **98,** 1372 (1993).
[68]A. D. Becke, *J. Chem. Phys.* **98,** 5648 (1993).
[69]C. Lee, W. Yang, and R. G. Parr, *Phys. Rev. B* **37,** 785 (1988).
[70]M. J. Frisch, G. W. Trucks, H. B. Schlegel, P. M. W. Gill, B. G. Johnson, M. W. Wong, J. B. Foresman, M. A. Robb, M. Head-Gordon, E. S. Replogle, R. Gomperts, J. L. Andres, K. Raghavachari, J. S. Binkley, C. Gonzalez, R. L. Martin, D. J. Fox, D. J. Defrees, J. Baker, J. J. P. Stewart, and J. A. Pople, G92/DFT, *Revision* G.3, (Gaussian, Inc., Pittsburgh, 1993).
[71]E. Kraka, J. Gauss, and D. Cremer, *J. Chem. Phys.* **99,** 5306 (1993).
[72]T. Joseph, R. Steckler, and D. G. Truhlar, *J. Chem. Phys.* **87,** 7036 (1987).
[73]H. Furue and P. D. Pacey, *J. Phys. Chem.* **94,** 1419 (1990).
[74]*JANAF Thermochemical Tables*, edited by M. W. Chase, Jr., C. A. Davies, J. R. Downey, Jr., D. J. Frurip, R. A. McDonald, and A. N. Syverud (J. Phys. Chem. Ref. Data, Vol. 14, 1985).
[75]D. L. Baulch, C. J. Cobos, R. A. Cox, C. Esser, P. Frank, T. Just, J. A. Kerr, M. J. Pilling, J. Troe, R. W. Walker, and J. Warnatz, *J. Phys. Chem. Ref. Data* **21,** 441 (1992).
[76]K. A. Nguyen, M. S. Gordon, and D. G. Truhlar, *J.Am. Chem.Soc.* **113,** 1596 (1991).
[77]T. N. Truong and W. T. Duncan, TheRate program (Univeristy of Utah, Salt Lake City, 1993). More information on this program can be obtained from the web page, http://www.chem.utah.edu/mercury/TheRate/TheRate.html, or send an email to TheRate@mail.chem.utah.edu.

Reprinted from ACS Symposium Series No. 629
Chemical Applications of Density-Functional Theory
Brian B. Laird, Richard B. Ross, and Tom Ziegler, Editors
Published 1996 by the American Chemical Society